Algorithm for detecting micro-aneurysms in low-resolution color retinal images

G. Yang[†], L. Gagnon[‡], S. Wang[†], M.-C. Boucher[♯]

[†] Département de mathématique et d'informatique, Univ. de Sherbrooke, Sherbrooke, QC, J1K 2R1

[‡] Centre de Recherche Informatique de Montréal, 550 Sherbrooke Ouest, Montréal, QC, H3A 1B9

[♯]Département d'ophtalmologie, Hôpital Maisonneuve-Rosemont, 5689 Boul Rosemont, Montréal, QC, H1T 2H1

Abstract

Diabetic retinopathy is the most common cause of blindness in the industrial countries. The first symptoms related to this disease is the appearance of small reddish spots on the retina, called micro-aneurysms (MAs). In this paper, we propose a practical algorithm for detecting MAs in color retinal images. The algorithm is based on a combination of image processing techniques like top-hat transform, CFAR threshold and region growing for segmenting MAs, as well as geometric and color features extraction for distinguishing MAs from other small targets. The algorithm is especially designed for low-resolution images such that it can be used on low-cost ophthalmic imaging systems for mass screening program.

1 Introduction

The purpose of this paper is to report about a practical algorithm for detecting micro-aneurysms (MAs) in low resolution color retinal images. The approach is inspired by Spencer et al. [7] regarding MA detection in high-resolution angiographic films.

MAs are the earliest symptoms associated to the diabetic retinopathy disease. Diabetic retinopathy is the most common cause of blindness in the industrial countries. MAs are retina lesions that appear as small reddish spots on color retinal images. They can be treated easily with a laser. The conventional way of detecting MAs consists in pointing them manually on an image of the retina. This is, of course, very much time consuming and because of that, automatic counting and analysis procedure using image processing tools have been proposed by different authors [1][2][5][7][11]. Most of these techniques however, have been developed for high-resolution fluorescence angiographic films. The main limitations with such image modality are that (1) it necessitates pupil dilation as well as an injection of fluorine marker into the patient in order to highlight the lesions, (2) the images are grey-scale, which prevents the use of color features for the classification of MAs and (3) the images are on film, limiting the use of digital enhancement tools.

Recently, digital color fundus cameras that do not require pupil dilation (non-mydriatic digital cameras) have become available. These ophthalmic image acquisition systems are easy to operate and economically more suitable for mass screening of diabetic retinopathy. Of course, mass screening implies the analysis of a large number of images which add to the interest in the use of automatic image tools. Such tools should at least be able to (1) pre-screen the images to separate normal from affected eyes and (2) provide disease grading of clearly affected eyes, letting medical specialists focus on doubtful cases.

Thus, low resolution digital color retinal images are the type of ophthalmic images we are interested in for this work. Figure 1 shows an example of such image from our image dataset. The image has a resolution of 20 μm/pixel, which is enough to detect most MAs (MA diameter varies between 5 and 125 μm).

The paper is organized as follows. Details about the algorithm, together with some intermediate results, are presented in the next section. Section 3 discusses some issues regarding the determination of the optimal parameters and the performance evaluation. Finally, summary and comments about possible improvements are given in the last section.

2 Presentation of the algorithm

The algorithm proceeds according to the following steps:

1. Preprocessing
2. Morphological filtering
3. Thresholding

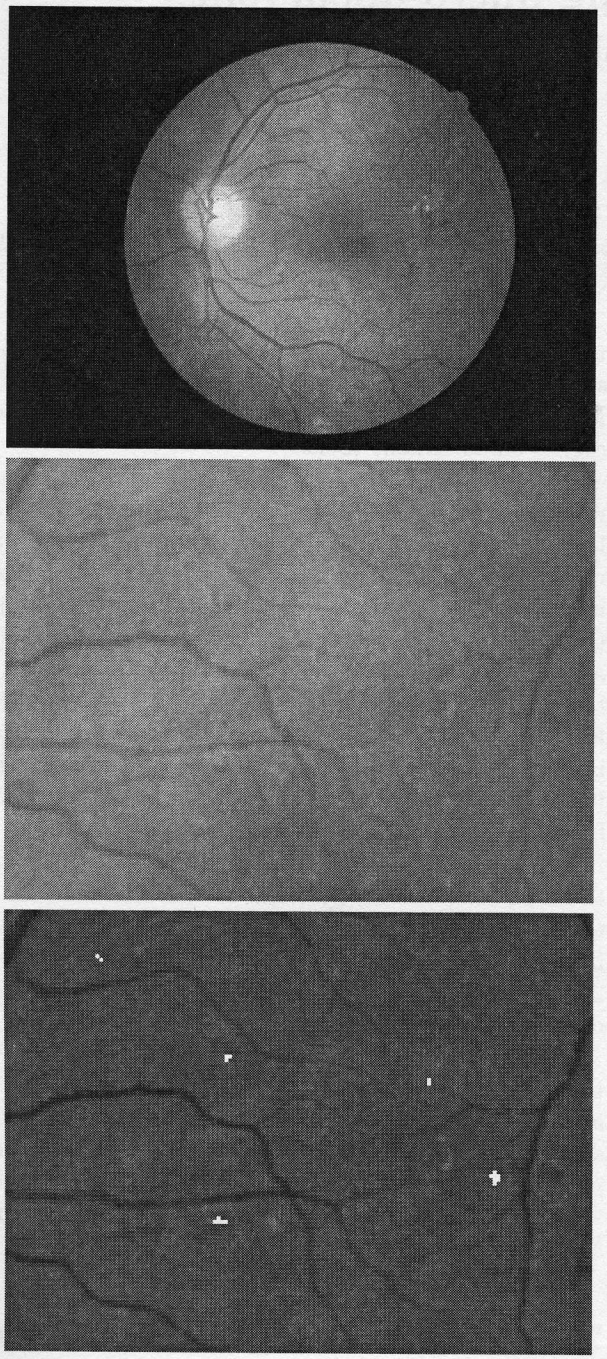

Figure 1: Example of a low resolution color retinal image (top) with an enlarged portion (middle) showing the presence of at least 5 MAs, and their detection with our algorithm (down).

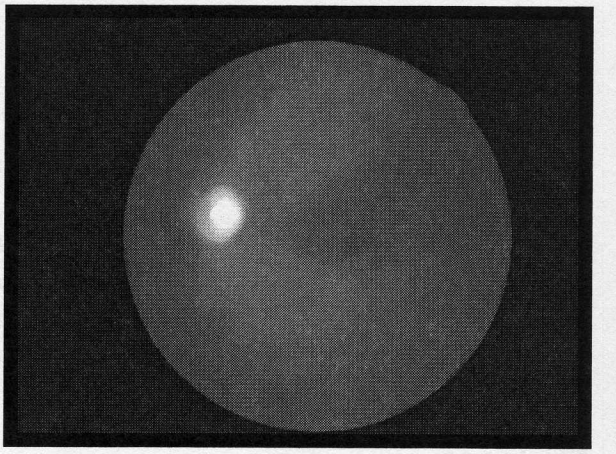

Figure 2: Example of a smoothed background green band image.

4. Region growing

5. Feature extraction and classification

Steps 1 to 4 are designed to extract candidate MAs on the green band of the color image. The main purpose of step 1 is to correct for the non-uniform illumination of the image. In step 2, a top-hat transform is used to make an initial segmentation of the image. The morphologically-transformed image is then thresholded in step 3 to generate a binary image containing candidate MAs. In step 4, a region-growing algorithm is applied to find the area of each marked object. Finally in step 5, the size, shape and color features of the candidate targets are analyzed to yield the final classification of MAs and, possibly, small round hemorrhages.

2.1 Preprocessing

First, a mask is built to focus on the center of the image [3], excluding the optic disk region [4]. Second, the green band of the image is extracted. Although MAs appear as reddish targets, it turns out that they are more distinguishable from the background in the green band image. Third, a non-uniform illumination correction is performed to compensate for the variation of the optical retina response or the non-uniformity of the imaging system. The compensated-image is obtained by dividing the green band image by an over-smoothed version of it (using a spatially large median filter). Figures 2 and 3 show examples of a smooth background image and the corresponding non-uniform illumination compensated image. The illumination-compensated image is the input of the next step.

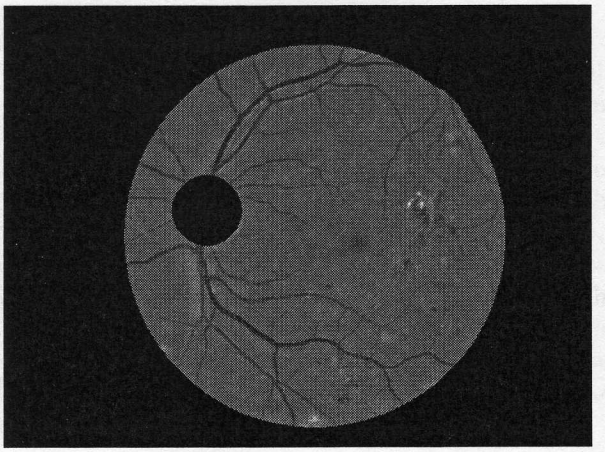

Figure 3: Example of a non-uniform illumination compensated green band image.

2.2 Morphological filtering

This step aims at isolating small dark circular objects in the green band image. This cannot be based on color characteristics since MAs and vessels are of similar colors. To separate them, one has to consider geometric properties; vessels are linear features while MAs are circular ones. Here, a top-hat transform is applied involving a geodesic reconstruction operation.

2.2.1 Top-hat transformation

Top-hat filtering is based on the idea of combining morphological opening and closing to extract peaks in signals [8]. The basic White Top-Hat (WTH) filter of an image I is the difference between I and its opening

$$I_{WTH} = I - I_{Open} \quad (1)$$

The shape and size of the structuring element depend on the form of the structures to be extracted. The WTH transformation can be used to remove objects similar to the structuring element in I. In our case, one wants to remove everything except small circular objects in the image. Since small vessels appear as linear structures in all possible directions, linear structuring elements at various orientation are used and applied as follows

$$I_{WTH} = I - max\{I_{Open}|\theta = 0, 15°, \ldots, 165°\} \quad (2)$$

In Eq. 2, θ is the orientation of the linear structuring element. The length of the structuring element should be slightly greater than the diameter of the largest circular feature to be segmented.

2.2.2 Geodesic reconstruction

After the top-hat transform, the image contains (in principle) no linear structures. However, there are small curved vessels that might not be removed by the top-hat transform. The reason is that the linear structuring element is sometimes too long to fit the small curved vessel. Thus, the opened image might not only eliminate the circular features but also some small curved vessels [11]. In order to recover these linear features, a geodesic reconstruction by dilation has been applied [8][11].

A geodesic dilation always involves two images, where the first image is dilated by an elementary isotropic structuring element and forced to be "lower" than the second image. This means that the second image acts as a limit to the propagation of the dilation on the first image [8]. In our case, one wants to recover some small vessels from the opened image. To this aim, we apply a geodesic reconstruction by dilating the opened image conditionally to the input top-hat image. The structuring element is a 3x3 square and the reconstructed image is used to replace the opened image in Eq. 2. Figure 4 shows the difference between a normal and geodesic reconstructed top-hat transform. Images have been enhanced by histogram equalization for display purpose. From these images we see that geodesic reconstruction reduces the number of false circular objects associated to small curved vessels.

2.3 Thresholding

The morphologically filtered image I_{Morph} obtained from the previous step has black background and bright (circular) targets. A typical histogram of such image is shown in Figure 5.

The bright targets are located at the tails of the histogram. This amounts to the use of Constant False Alarm Rate (CFAR) techniques for separating background and potential targets. A conventional exponential-CFAR thresholding techniques (see for instance [6] and references therein) have been considered but they tend to provide unstable detection results (too many targets detected on one image, too few on another one). Of course, we could have set the threshold to a very low level in order to get a high detection rate (even at the expense of increasing the false detection rate), but this would have made subsequent target analyses more difficult. We preferred to optimize the thresholding step as much as possible.

We found that the thresholding formula

$$Thresh = \alpha m_2 \quad (3)$$

provides the best result. In Eq. 3, α is a free parameter and m_2 is the second order moment of the histogram

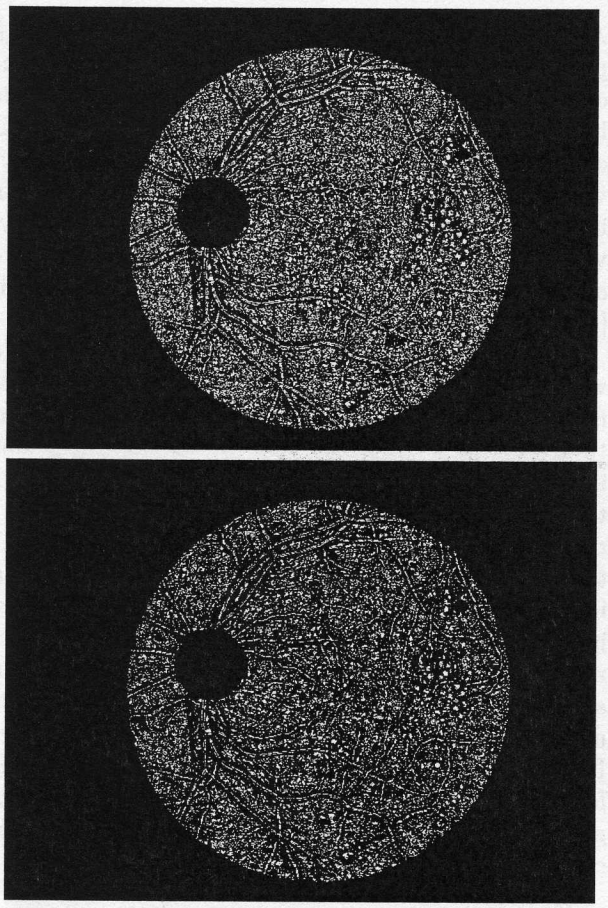

Figure 4: Example of top-hat transformed images without (top) and with (down) geodesic reconstruction

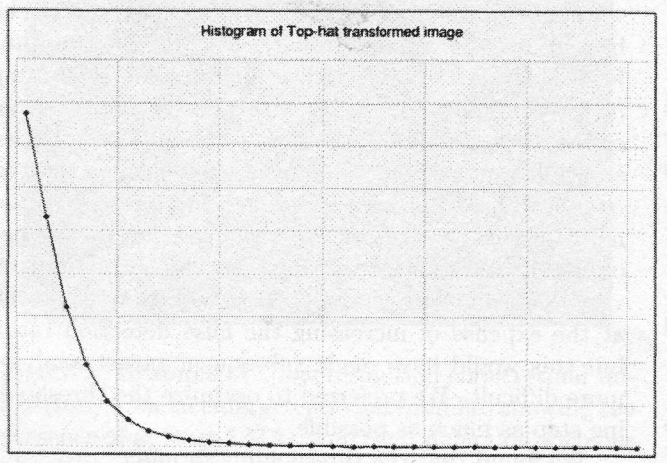

Figure 5: Example of histogram for a typical top-hat transformed image.

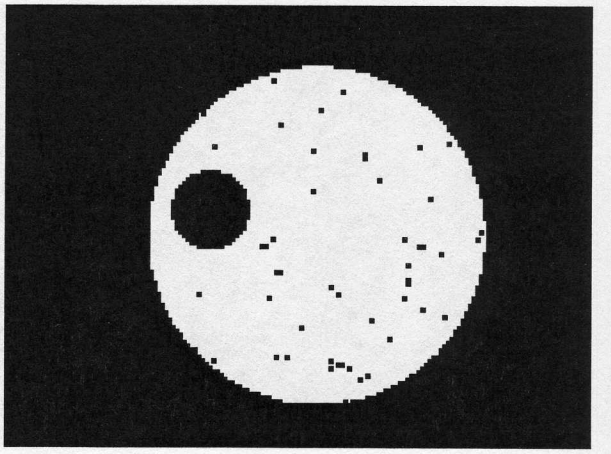

Figure 6: Example of thresholded top-hat image showing pointers (black dots) to candidate MAs for the next characterization step.

$h_{I_{Morph}}$ of I_{Morph}. This heuristic thresholding formula is based on the experimental observation that the number of MAs present in the morphological filtered image is approximately proportional to m_2.

In fact, we also found that the number of MAs is also proportional to the squared root of the fourth order moment m_4. This leads to the following justification about the choice of 3. It is well known that the fourth central moment (kurtosis) of a distribution is a typical measure of the flatness of the density function. For an image, if most pixel values are above the mean grey level value, then the histogram kurtosis is large. From $h_{I_{Morph}}$, we build a symmetrical histogram h'centered at zero such that

$$h'(k) = \begin{cases} h_{I_{Morph}}(k) & \text{for } k \geq 0 \\ h_{I_{Morph}}(-k) & \text{for } k < 0 \end{cases} \quad (4)$$

The kurtosis of $h'(k)$, noted μ_4, can be used to compute the threshold for I_{Morph}. In our experiments, $Thresh = \beta\sqrt{\mu_4}$ has proved to be efficient since it allows trade-off between high detection rate and low false alarm rate with a constant coefficient β for all images in the dataset. In practice however, we rather used Eq. 3 because it is approximately equivalent to $Thresh = \beta\sqrt{\mu_4}$. In fact, μ_4 is the same as m_4 for $h_{I_{Morph}}$ and since $h_{I_{Morph}}$ follows approximately an exponential distribution $(\lambda * exp(-\lambda x))$, one has $m_4 \doteq 6m_2^2$, and thus $Thresh = \beta\sqrt{\mu_4} \doteq \beta\sqrt{6}m_2$.

At the end of this step, the objects in the thresholded binary image are pointers to candidate MAs and, along with the original gray-scale image, represent the input data for the next region-growing algorithm (Figure 6).

2.4 Region growing

Region growing is a procedure that groups pixels or subregions into larger regions. Merging is done according to similarity constraints starting from a seed pixel (or a seed area). In our algorithm, region-growing is used to delineate and fill-in the object area marked by the pixels passing the threshold test of the previous step.

The seeds are selected by looking over the small connected region in the binary image and by retaining the pixel with the lowest grey level in the corresponding original green band image. From that seeds, one uses the following criterion to include the neighbors pixel into the growing object [7] :

$$i \leq i_{seed} + x(i_{bgnd} - i_{seed}) \quad (5)$$

In Eq. 5, i is the grey-level of the pixel under test, i_{seed} is the grey-level of the single-pixel seed, i_{bgnd} is the grey-level of the background image at the same spatial position and x is a region growing parameter with value between 0 and 1. The procedure stops when condition 5 is not satisfyed or by a control mechanism that test if the grown region exceeds a predefined size. (This sometimes happens if the seed pixel belongs to a vessel).

2.5 Classification

Objects in the region grown image are analyzed to identify MAs using various geometrically-based or color-based features. These include the maximum and minimum value of the object perimeter, the aspect ratio, the shape complexity and the hue.

2.5.1 Geometrical features

The geometrical features we use are the area, aspect ratio and shape complexity. An upper limit is set for the area of candidate MAs. Small targets containing 1 or 2 pixels are automatically retained as a potential MA and sent to the color feature module. If larger circular lesions need to be detected (i.e. round hemorrhages), a minimum value can be given.

The shape complexity is evaluated using the circularity $C = \frac{perimeter^2}{4\pi * area}$. In the continuous space, a circle has a (minimum) circularity value of 1. In a digital image however, the circularity can has value less than 1. An upper limit has been set to ensure that a target having a capillary tail attached to them or with a slightly irregular shape is excluded at this stage.

The aspect ratio, defined as the target height-to-width ratio, is also used to quantify the target shape. To this aim, one calculates the target's centroid and orientation in order to determine the target's longest and shortest dimensions. In principle, aspect ratio of MAs should be unity. However, many of them are elongated in some way in low resolution images. A lower limit on the aspect ratio is set to tolerate these deviations from the ideal case.

2.5.2 Color feature

The color feature we use is the hue, represented as an angle on the color circle. By definition $Red = 0°$ and the other colors are spread around the circle (e.g. Green=120°, Blue=240°, etc.). The measure of the target redness (low hue value) is used to make the final decision on whether a target is a MA or not. A dynamic thresholding approach has been implemented in order to cope with the fact that retinal color varies from person to person. We use a Gaussian CFAR thresholding method to adaptively adjust the detection threshold between images. The mean hue P over a potential MA is calculated and the target is declared as a true MA if P satisfies

$$P < \mu - \alpha \cdot \sigma \quad (6)$$

where μ and σ are the global mean and the standard variation of the hue image and α is a free hue threshold parameter.

3 Results

3.1 Parameters optimization

Some of the free parameters defined above can be set on the basis of known *a priori* physical constraints or by performing tests on artificial images. These are the structuring element length of the top-hat transform, the upper and lower limits of the target area, the lower limit of the target complexity (circularity) and the lower limit of the target aspect ratio.

The length of the structuring element and the upper limit on the target area are related and set by the size of the MA and the resolution of the imaging system. Since the maximum dimension of MAs is about 125μm and the resolution of the imaging system is about 20 μm/pixel, the structuring element length has been set to 7. In order to set the range of the complexity measure and of the aspect ratio, target shape characteristics containing 3, 4 and 5 pixels have been carefully studied. To this aim, an artificial image with a grey-level background (127) and with white targets (255) has been used as input to the program. An analysis of the complexity and aspect ratio for these artificial targets led to the wanted criteria. Details can be found in [10].

The other free parameters must be optimized using ground truth images. These are the threshold level and the upper limit of the mean target hue value. Next section describes the procedure we used.

3.2 Detector performance

It is impossible in this type of application to get a perfectly reliable ground truth on real images. Even medical experts may fail identifying all MAs in an image. This implies that direct statistical evaluation is very difficult to realize in practice. To overcome this difficulty, while getting a general idea of the detector performance, we have used a test procedure very popular in satellite imagery. It relies on the insertion of known targets in real "background" images and on the analysis of ROC curves (see for instance [9] and references therein).

Small chips images of 7x7 pixels containing only one true MA have been extracted from fundus images of diabetic patients and inserted into normal fundus images. In this way, the number and position of all MAs is known exactly. The difficulty of the task however is to smoothly insert targets to make their appearance as natural as possible. To this aim, we first calculate the background of the chips and insert them by matching that background with the local background of the "background" image.

ROC curve analysis is then used to establish the optimal relationship between the sensitivity (the ability to detect a true MA when it is present) and the false alarm rate. The sensitivity (detection rate) is defined as

$$Sensitivity = \frac{TP}{TP + FN} \tag{7}$$

where TP and FN are the number of true positives and false negatives, respectively.

Three images of healthy retina, in which hundreds of true MAs were inserted, have been used to build ROC curves. Result is shown on Figure 7. Each curve corresponds to a different region growing parameter (circles: 60%, squares: 50%, triangles: 40%). Each point on the curves corresponds to a different value of the thresholding parameter α. The color feature (hue) has not been included during that test. In Figure 7, we see that the maximum sensitivity achieved by the detector is about 90% and that the best trade-off is about 80% sensitivity and 10% false alarm for a region growing parameter of 50%. The fact that the detector cannot reach the maximum sensitivity of 100% means that some true targets are always discarded on the base of their shape analysis. This is a consequence of the choice we have done for the lower and upper limit values for the circularity and aspect ratio. In fact, this goes back to the problem of using such geometric features on targets of very few pixels. It is clear that further improvements are necessary on that side.

Tests on a bank of 46 real images (of normal and sick eyes of various visual quality) acquired from a digital non-mydriatic camera (Canon CR6-45NM) have also been performed but detailed results cannot be reported at this time. However, we have been able to set up the algorithm parameters to ensure 90% of "global" sensitivity (i.e. the ability to detect at least one MA in a true sick eye) on these real images while keeping a high value (up to 80%) for the "global" specificity (i.e. the ability of not detecting any MA on an healthy eye). From a clinical point of view, 90% and 80% of global sensitivity and specificity are significant because it means that 90% of the sick persons would be referred to a specialist without to much overloading their tasks with healthy persons (20%). Of course, the targeted medical performance for such algorithm is 100% sensitivity and 100% specificity; which still leaves room for improvements.

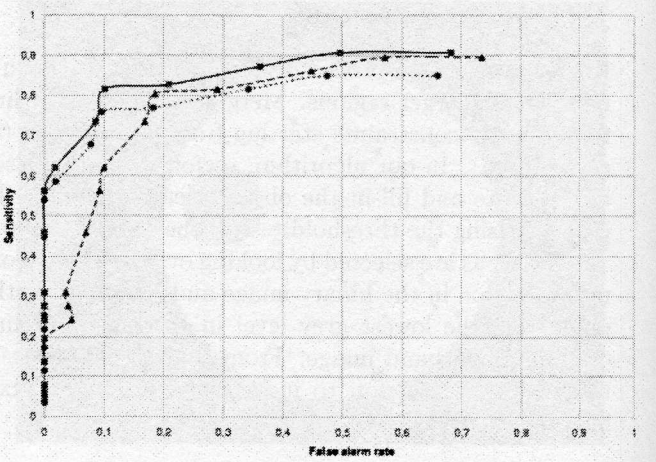

Figure 7: ROC curves for three values of the region growing parameters (circles: 60%, squares: 50%, triangles: 40%)

Finally, processing one image takes about 15 seconds on a Pentium II - 300 MHz processor.

4 Summary and comments

We have presented an algorithm for the detection of micro-aneurysms (MAs) in low resolution color retinal images. The procedure is an adaptation of a MA detector developed for high-resolution angiographic films [7]. Designing a MA detector that works on digital low-resolution color images rather than angiographic grey-level films is more attractive in the context of mass screening of diabetic retinopathy which requires fast and economic diagnosis systems to operate. The solution presented here is not perfect but it provides a good compromise for automatic pre-screening of sick and healthy eyes.

Of course, the procedure can be improved in many

ways: faster image preprocessing and morphological implementation, more accurate statistical models, texture-based region growing, improvement of the geometric-based features and, possibly, addition of other ones. However, one has to keep in mind that real-time diagnosis is not critical in this type of medical application and that detecting all MAs in a retinal image is not a requirement to diagnose diabetic retinopathy disease. Thus, for mass screening, we believe the algorithm is efficient enough for practical use.

Finally, it is more likely that resolution of non-mydriatic digital cameras will increase in the future, while the system cost will remain stable or even decrease. We believe that our algorithm, which is already performing well for detecting dim targets on low resolution imagery, should perform even better on higher-quality images.

Acknowledgments

GY acknowledges financial support from CRIM and Université de Sherbrooke. Research works of LG and SW are supported in part by grants from the Natural Science and Engineering Research Council (NSERC) of Canada. LG and MCB acknowledge support from the Canadian Foundation for Innovation.

References

[1] M. J. Cree, J. A. Olson, K. C. Mchardy, P. F. Sharp, and J. V. Forrester, "A fully automated comparative micro-aneurysm digital detection system," *Eye*, Vol. 11, pp. 622-628, 1997.

[2] A. J. Frame, P. E. Undrill, M. J. Cree, J. A. Olson, K. C. Mchardy, P. F. Sharp, J. V. Forrester, "A comparison of computer based classification methods applied to the detection of micro-aneurysms in ophthalmic fluorescein angiograms", *Computers in Biology and Medicine*, Vol. 28 pp. 225-238, 1998.

[3] L. Gagnon, M. Lalonde, M. Beaulieu, M.-C. Boucher, "Procedure to detect anatomical structures in optical fundus images", *Proceedings of the SPIE Conference on Medical Imaging: Image Processing* (SPIE #4322), San Diego, 2001 (to appear)

[4] M. Lalonde, M. Beaulieu, L. Gagnon, "Fast and robust optic disk detection using pyramidal decomposition and Hausdorff-based template matching", CRIM report CRIM-00/12-11, submitted to *IEEE Trans. on Medical Imaging*

[5] A. M. Mendonça, A.J. Campilho, J.M. Nunes "Automated Segmentation of Micro-aneurysms in Retinal Angiograms of Diabetic Patients", *Proceedings of 10th International Conference on Image Analysis and Processing*, pp. 728-733 Venice, Italy, 1999.

[6] R. Ravid, N. Levanon, "Maximum-Likelihood CFAR for Weibull Background", *IEE Proceedings-F*, Vol. 139, pp. 256-264, 1992

[7] T. Spencer, J. A. Olson, K. C. Mchardy, P. F. Sharp, J. V. Forrester, "An image-processing strategy for the segmentation and quantification of micro-aneurysms in fluorescein angiograms of the ocular fundus", *Computers and biomedical research*, Vol. 29, pp. 284-302, 1996.

[8] P. Soille, *Morphological Image Analysis: Principles and Applications,* Spinger, 1999.

[9] N. S. Subotic, B. J. Thelen, J. D. Gorman, M. F. Reiley, "Multiresolution Detection of Coherent Radar Targets", *IEEE Trans. Image Processing*, Vol. 6, pp. 21-35, 1997

[10] G. Yang, "Detection of micro-aneurysms in low resolution color retinal images", *Master Thesis*, Under preparation, 2001.

[11] F. Zana, I. Meunier, J. C. Klein, "A region merging algorithm using mathematical morphology: application to macula detection", *Proceedings of DSP 97*, pp. 1087-1091, 1997.